Evolution of the anemone AR NOAA 10798 and the related geo-effective flares and CMEs

Ayumi Asai,[1,2,3] Kazunari Shibata,[4] Takako T. Ishii,[4] Mitsuo Oka,[4,5] Ryuho Kataoka,[6] Ken'ichi Fujiki,[7] and Nat Gopalswamy[8]

Received 9 April 2008; revised 10 November 2008; accepted 17 December 2008; published 21 February 2009.

[1] We present a detailed examination of the features of the active region (AR) NOAA 10798. This AR generated coronal mass ejections (CMEs) that caused a large geomagnetic storm on 24 August 2005 with the minimum Dst index of −216 nT. We examined the evolution of the AR and the features on/near the solar surface and in the interplanetary space. The AR emerged in the middle of a small coronal hole, and formed a sea anemone like configuration. Hα filaments were formed in the AR, which have southward axial field. Three M class flares were generated, and the first two that occurred on 22 August 2005 were followed by Halo-type CMEs. The speeds of the CMEs were fast, and recorded about 1200 and 2400 km s^{-1}, respectively. The second CME was especially fast, and caught up and interacted with the first (slower) CME during their travelings toward Earth. These acted synergically to generate an interplanetary disturbance with strong southward magnetic field of about −50 nT, which was followed by the large geomagnetic storm.

Citation: Asai, A., K. Shibata, T. T. Ishii, M. Oka, R. Kataoka, K. Fujiki, and N. Gopalswamy (2009), Evolution of the anemone AR NOAA 10798 and the related geo-effective flares and CMEs, *J. Geophys. Res.*, *114*, A00A21, doi:10.1029/2008JA013291.

1. Introduction

[2] Space weather has attracted a lot of attention in recent times. Space weather research involves various related fields, such as the solar surface, solar wind, interplanetary space, geomagnetosphere, ionosphere, and atmosphere, since a comprehensive understandings from active phenomena on the solar surface to the propagation of the disturbances toward Earth are crucially required for the studies.

[3] Vast plasma ejected from the solar corona in the form of coronal mass ejections (CMEs) leads to a geomagnetic storm, and therefore, CMEs have been actively discussed. Moreover, large geomagnetic storms are associated with large flares (that are emitting strong X ray), long duration events (LDEs), fast CMEs, and so on [e.g., *Gopalswamy et al.*, 2007]. Flare locations are another factor for a major geomagnetic storm, since the flare location close to the disk center indicates that the related CME is heading towards Earth and is likely to cause a large geomagnetic storm [*Manoharan et al.*, 2004]. Ejections that cause strong disturbances with southward magnetic field in the interplanetary space are also important. Coronal holes (CHs) are, on the other hand, related with fast solar wind because of their open magnetic field, and therefore, themselves have been another important factor for space weather studies. While large geomagnetic storms are caused by Earth-directed CMEs [see, e.g., *Gosling et al.*, 1990], weaker storms are associated with high-speed streams from CHs [see, e.g., *Sheeley et al.*, 1976]. However, storms related to high-speed streams from CHs cause larger flux enhancement of MeV electrons of the Earth's Van Allen belt than the CME-associated storms do on average [*Kataoka and Miyoshi*, 2006]. It has been, furthermore, reported that many fast Halo CMEs are associated with CHs [*Verma*, 1998; *Liu and Hayashi*, 2006]. The recent work done by *Liu* [2007] showed that the speeds are faster even statistically than those of CMEs under the heliospheric current sheet. Therefore, in order to understand what kind of events can generate a large geomagnetic storm, it is necessary to study active phenomena on the solar surface and the propagation in the interplanetary space, in relation to the surrounding magnetic structure. In this paper we examine in detail the evolution of an active region (AR) that emerged in a CH and the related flares, CMEs, and the geomagnetic storm to elucidate how such a magnetic configuration works to generate a geo-effective flares/CMEs.

[4] CMEs originating from AR NOAA 10798, generated a large geomagnetic storm on 24 August 2005, which was one of the 88 major geomagnetic storms reported by *Zhang et al.* [2007]. This AR has been highly paid attention to, since it was one of the targets of the International CAWSES (Climate and Weather of the Sun-Earth System) Campaign (see http://www.bu.edu/cawses/secondcampaign.html), and at the related virtual conference (http://workshops.jhuapl.

[1]Nobeyama Solar Radio Observatory, National Astronomical Observatory of Japan, Minamisaku, Japan.
[2]National Astronomical Observatory of Japan, Mitaka, Japan.
[3]Graduate University for Advanced Studies, Hayama, Japan.
[4]Kwasan and Hida Observatories, Kyoto University, Yamashina, Japan.
[5]Center for Space Plasma and Aeronomic Research, University of Alabama in Huntsville, Huntsville, Alabama, USA.
[6]RIKEN, Wako, Japan.
[7]Solar-Terrestrial Environment Laboratory, Nagoya University, Nagoya, Japan.
[8]NASA Goddard Space Flight Center, Greenbelt, Maryland, USA.

Copyright 2009 by the American Geophysical Union.
0148-0227/09/2008JA013291

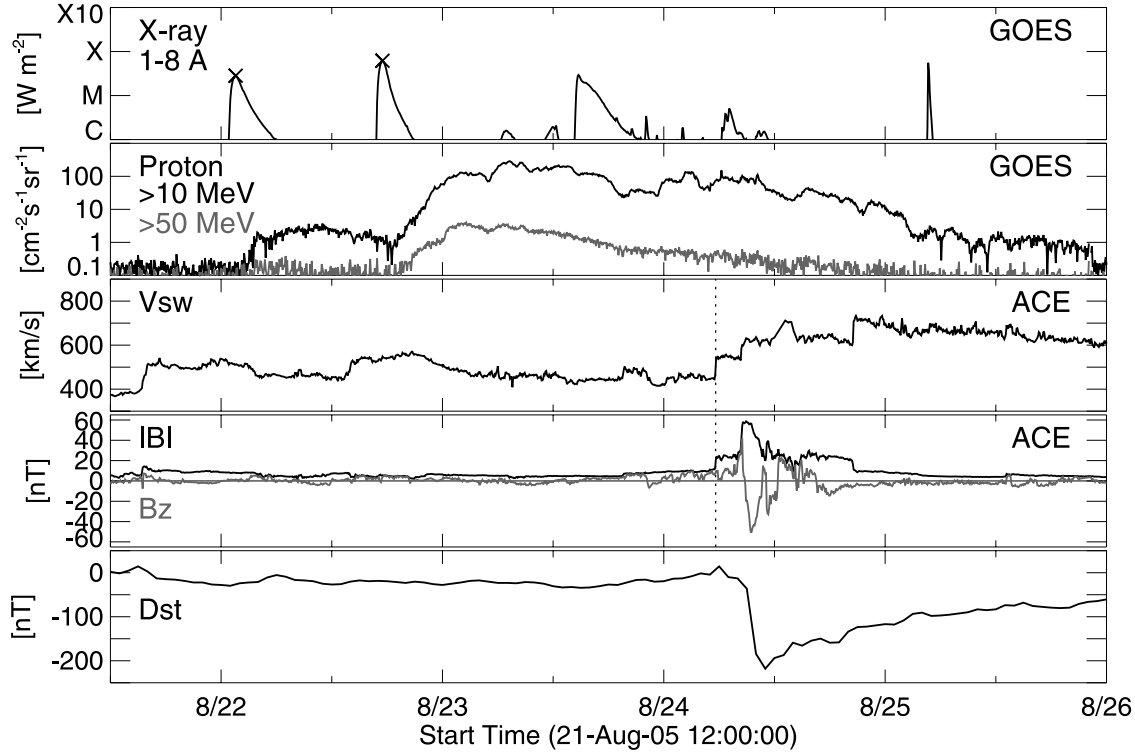

Figure 1. Overview of the geomagnetic storm that occurred on 24 August 2005 and the related solar-terrestrial events. (top to bottom) SXR flux in the GOES 1.0–8.0 Å channel, proton fluxes in >10 MeV (black line) and >50 MeV (gray line) channels obtained with GOES, bulk velocity of solar wind V_{sw} measured with ACE, total magnetic field strength $|B|$ (black line) and Z component of the magnetic field B_z (gray line) measured with ACE, and Dst index produced by the Kyoto University.

edu/s1/index.html), there were intensive discussions on the AR [e.g., *Asai et al.*, 2006]. Figure 1 shows an overview of the geomagnetic storm and the related solar-terrestrial events. The Soft X-ray (SXR) flux in the GOES 1.0–8.0 Å channel shows three M class flares that occurred on 22 and 23 August 2005. The first two flares (marked with crosses) were associated with the CMEs responsible for the geomagnetic storm in question. In the second panel we can recognize the sufficient enhancements of the proton fluxes in >10 MeV (black line) and >50 MeV (gray line) channels obtained with GOES. Both flares were followed by enhancements of solar energetic particles (SEPs), and the second flare's was larger. The bulk velocity of solar wind V_{sw} in the third panel and the total $|B|$ (black line) and Z component of the magnetic field B_z (gray line) in the fourth panel were measured with the Advanced Composition Explorer (ACE). The first shock was recorded at 05:35 UT by ACE as shown by the dashed line. The same shock was also recorded by the Geotail satellite at 06:15 UT. The interplanetary magnetic field had a strong southward component of about −50 nT. The bottom panel shows the Dst index produced by the Kyoto University. The decrease of the Dst index was quite large, reaching −216 nT. In section 2 we describe the evolution of the AR, focusing on the photospheric magnetic configuration, and the Hα filament formed during the evolution of the AR and the coronal features are also presented. In section 3 we discuss the flares/CMEs that occurred on 22 August 2005. In section 4 we shortly review the associated interplanetary disturbances. In section 5 we summarize our results.

2. Evolution and Structure of Active Region NOAA 10798

2.1. Evolution

[5] First, we examine the evolution of the photospheric magnetic field. Figure 2 shows the continuum images (top), the magnetograms (middle), and the extreme ultraviolet (EUV) images (bottom) of AR NOAA 10798. The continuum images and the magnetograms were obtained with the Michelson Doppler Imager (MDI [*Scherrer et al.*, 1995]) aboard the Solar and Heliospheric Observatory (SOHO [*Domingo et al.*, 1995]), while the EUV images are taken with the Extreme-Ultraviolet Imaging Telescope (EIT [*Delaboudiniére et al.*, 1995]) aboard SOHO. Each image was taken at about 00:00 UT of the day. AR NOAA 10798 emerged on 18 August 2005 and rapidly evolved.

[6] Although the region showed a simple bipolar configuration, while it was in violation of the so-called "Hale-Nicholson's magnetic polarity law" [*Hale et al.*, 1919], according to which the preceding spots in the southern hemisphere should have a negative polarity during solar cycle 23. These "reverted polarity" ARs are statistically more likely to generate flares and CMEs [*López Fuentes et al.*, 2003; *Tian et al.*, 2005]. We checked all the ARs that appeared in 2005, and found that only 7 ARs (5%), including the AR NOAA 10798, were the "reverted polarity"

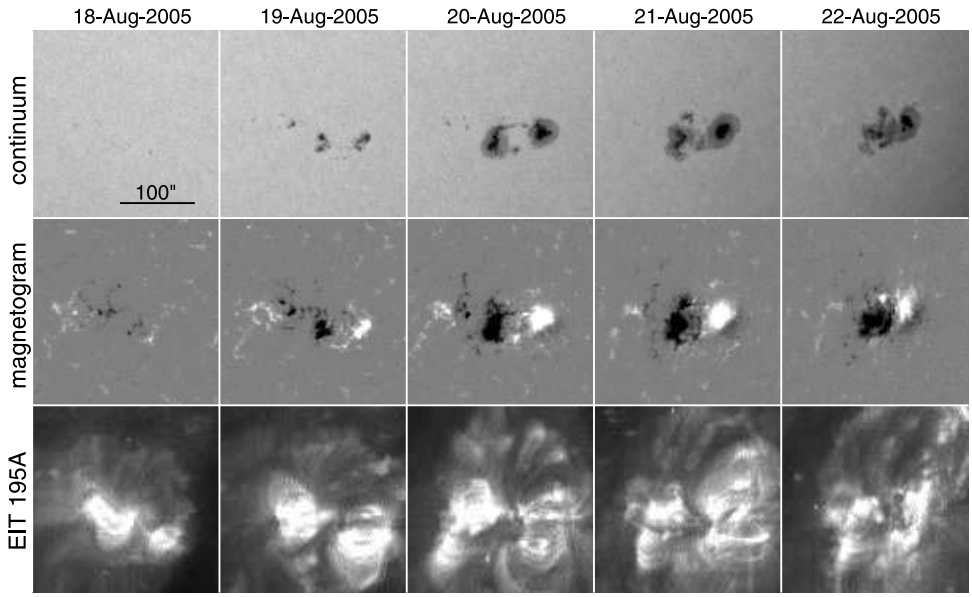

Figure 2. Temporal evolution of the AR. The (top) continuum images and the (middle) magnetograms observed by SOHO/MDI. (bottom) The EUV images obtained with SOHO/EIT. Each image was taken at about 00:00 UT of the day. Solar north is up, and west is to the right.

ARs. Furthermore, 4 of the 7 ARs, including AR NOAA 10798, showed high solar activity. This implies that AR NOAA 10798 had potentially a very complex structure. For example, a highly twisted and kinked magnetic structure may be embedded beneath the photosphere as *Ishii et al.* [2000] and *Kurokawa et al.* [2002] reported. Indeed, we can see the rotating motion of the pair of the sunspots counter-clockwise during the disk passage. This AR further evolved and generated an X17 flare on 7 September 2005 when it returned as AR NOAA 10808 [*Wang et al.*, 2006; *Nagashima et al.*, 2007].

[7] The top panel of Figure 3 shows the SXR lightcurves obtained by GOES in the 1.0–8.0 Å (upper) and 0.5–4.0 Å (lower) channels. The bottom panel of Figure 3 shows the time profiles of the magnetic flux of this AR. That for the negative magnetic flux is multiplied by -1. The calculated area is $400'' \times 400''$, and is as wide as it covers the whole AR. Following the emergence and evolution of the active region from 18 August 2005, the magnetic fluxes as well as the SXR intensity gradually increased, with three M class flares occurring on 22 and 23 August, before rotating behind the west limb. In this paper we mainly discuss the first two flare that occurred on 22 August 2005, since the geomagnetic storm on 24 August 2005 is attributed to the related eruptions/CMEs.

2.2. Filament Formation

[8] Second, we examine the filament formation in AR 10798, using the Hα images. A filament is just a visualized part of a helical flux rope, and it is only a fraction of the whole of the flux rope. However, it is thought that a filament is located in the middle of the flux rope, and that it even represents the whole structure [see, e.g., *Low and Hundhausen*, 1995]. Therefore, an eruption of a filament is always related with a large-scale disturbance of the coronal magnetic field that often appears as an EIT dimming. As *Munro et al.* [1979] suggested that more than 70% of CMEs are associated with eruptive prominences or filament disappearances (with or without flares), and therefore, filament eruptions are very important as a CME-associated phenomenon. Moreover, we often see an ejected filament observed in Hαs/microwaves or a plasmoid in SXRs at the center of an ejecta, when it is accompanied by a flare. We can even roughly extrapolate the magnetic configuration of a CME from that of the ejected filament. For example, *Rust* [1994] showed that the helicity of ejected filaments correspond to the chirality of magnetic clouds passing Earth (about 4 days after the eruptions).

[9] Figure 4 shows the temporal evolution of the AR in the Hα images (top) and the magnetic field (bottom). The Hα images in Figures 4a and 4b were taken with the Solar Magnetic Activity Research Telescope (SMART) (http://www.hida.kyoto-u.ac.jp/SMART/) at Hida Observatory, Kyoto University. Figures 4c and 4d were obtained at the Observatoire de Paris, Section de Meudon, and the Big Bear Solar Observatory, respectively. Both of these images were obtained through the online data center of the Global High-Resolution Hα Network (http://www.bbso.njit.edu/Research/Halpha/). The magnetograms (Figues 4e–4h) were taken by SOHO/MDI.

[10] For three days after the emergence of the AR (until 20 August), a clear arch-filament system [*Bruzek*, 1967] was seen (Figure 4a). The bipole-like systems bridged the neutral line and connected the spots of opposite polarity. On the other hand, after 21 August 2005, these filamentary structure was abruptly changed. In Figure 4b, some oblique structure appeared, and showed prefilamental structure. Comparing with the magnetograms (Figure 4, bottom), we confirm that the magnetic field of these structure was oriented from northwest to southeast, which means they had southward magnetic field. About nine hours after this (Figure 4c), the sheared filamentary structure evolved to a large Hα filament that lay on the magnetic neutral line between the sunspots. The arrow in Figure 4c points to the

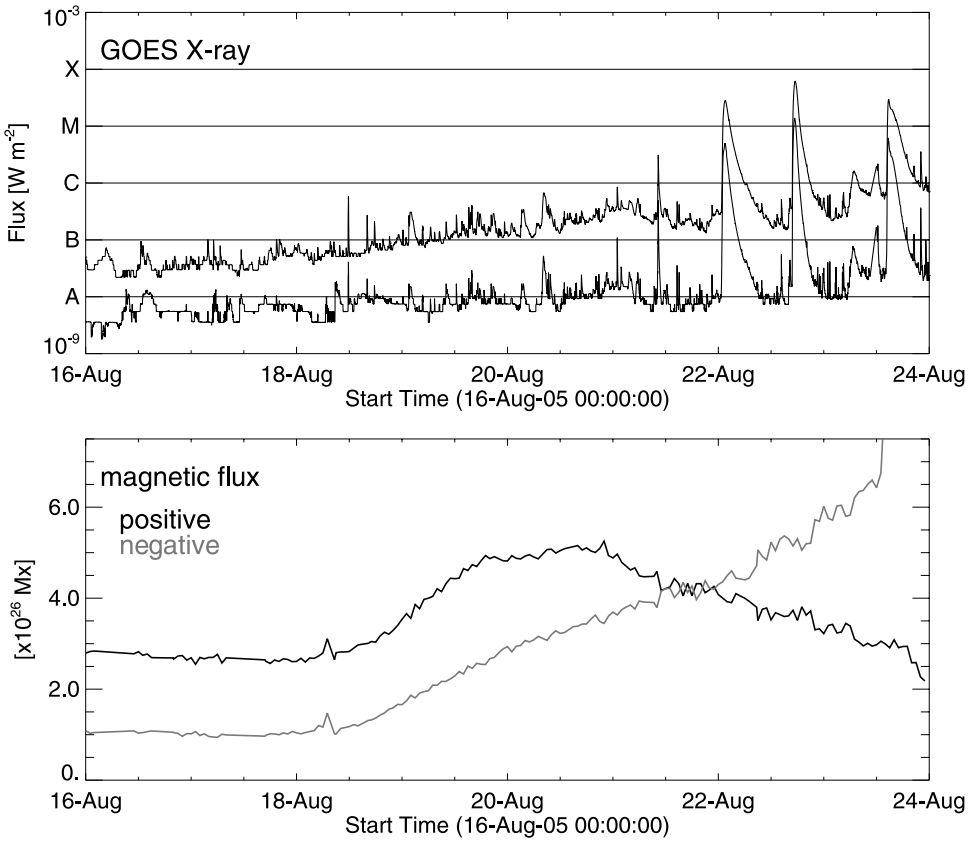

Figure 3. Time profiles of SXR flux and magnetic fluxes. (top) SXR flux in the GOES 1.0–8.0 Å (upper) and 0.5–4.0 Å (lower) channels. (bottom) Magnetic flux of the AR observed with SOHO/MDI. The calculated area is $400'' \times 400''$ centered on the middle of the AR, and is as wide as it covers the whole AR. The time profile of the negative magnetic flux is multiplied by -1.

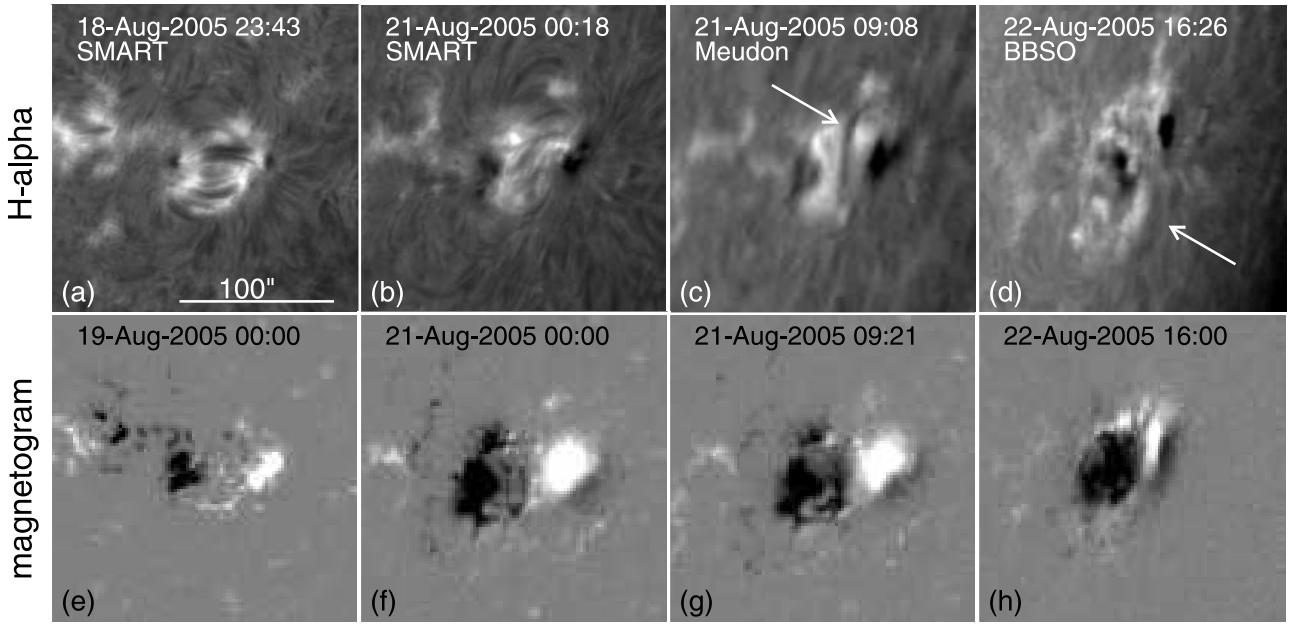

Figure 4. (top) Hα images. (a and b) Obtained with SMART at Hida Observatory, Kyoto University. (c and d) Obtained at Observatoire de Paris, Section de Meudon, and Big Bear Solar Observatory, respectively. (bottom) Magnetograms taken with SOHO/MDI.

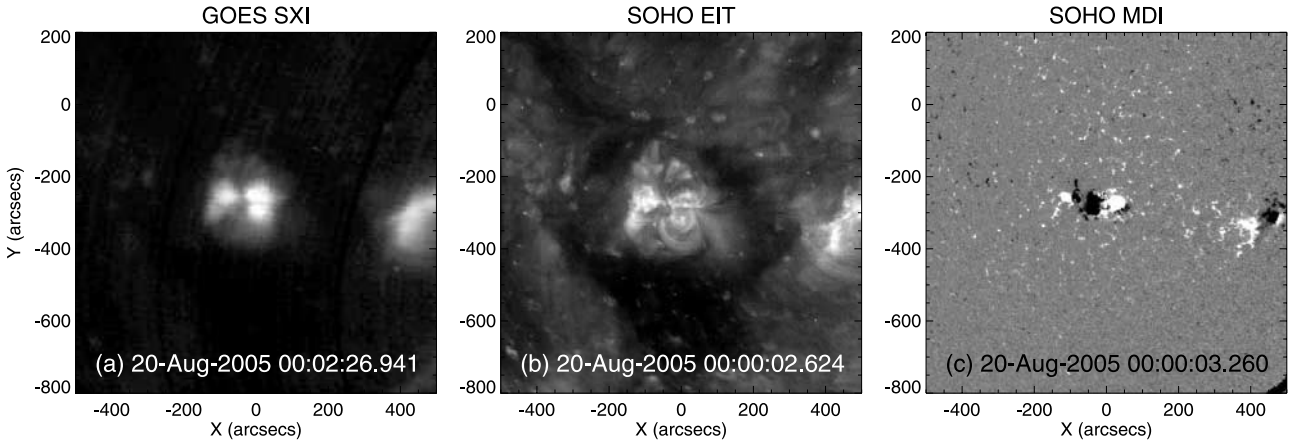

Figure 5. Coronal feature of AR NOAA 10798. (a) A SXR image obtained with GOES/SXI. (b) An EUV (195Å) image obtained with SOHO/EIT. The bright region near the center of the image is the AR. The surrounding dark region is a CH. (c) A magnetogram taken with SOHO/MDI.

filament. The filament formation is consistent with what *Martin* [1973] pointed out long ago: developed filaments usually become apparent about the "fourth day" after the initial formation of an active region. Unfortunately, there are no data between Figures 4b and 4c, but we can see the new flux emergence around the magnetic neutral line, (compare Figure 4f with Figure 4g). The formation of the filaments with the southward magnetic field is probably related to the emerging flux.

[11] The first M class flare occurred at 00:44 UT on 22 August 2005, which is in the middle of the time between Figures 4c and 4d. In Figure 4d, we can recognize the disappearance of the Hα filament after the first flare, while a new filament formed in the south part of the AR as pointed by the arrow in the panel. Associated with the first flare, the Hα filament formed in the northern part (Figure 4c) erupted, and with the second flare, the southern one (Figure 4d) erupted. The axial field of these filaments had southward magnetic field, which is easily inferred from the prefilamentary structure. Although we also checked the EUV data taken with EIT and the Transition Region and Coronal Explorer, we could not find out any phenomena that can be a source of the CMEs other than the filament eruptions. We will discuss the flares and CMEs in more detail in section 3.

2.3. Anemone Structure

[12] Figures 5a and 5b show the coronal structure of the AR observed at about 00:00 UT on 20 August 2005, in SXR and in EUV with Solar X-ray Imager (SXI) on board GOES and SOHO/EIT, respectively. The bright structure near the center of the image is AR NOAA 10798. Figure 5c shows the magnetogram taken by SOHO/MDI. The following sunspot with the negative (that is black) polarity is the center of the EUV bright structure, and a radial array of loops is formed. We also present schematic cartoons of the magnetic structure of AR NOAA 10798 in Figures 6a and 6b.

[13] The appearance is like a sea anemone, and this type of ARs is sometimes called "anemone structure" [*Shibata et al.*, 1994a, 1994b], or originally "fountain" [*Tousey et al.*, 1973; *Sheeley et al.*, 1975a] in the Skylab era. We call these ARs "anemone ARs" in this paper. These anemone ARs are often associated with the emerging fluxes within unipolar regions [*Sheeley et al.*, 1975b], and in most cases, they appear in CHs [*Asai et al.*, 2008]. Although characteristics of anemone ARs have been mainly discussed only in SXRs, they are commonly seen under such a magnetic configuration, even in a chromospheric line by the Solar Optical Telescope on board Hinode [*Shibata et al.*, 2007].

[14] As shown in Figure 5, AR NOAA 10798 is clearly surrounded with a unipolar region with the positive magnetic polarity, and shows the anemone appearance both in SXR and in EUV, and we can conclude that AR NOAA 10798 was a typical anemone AR. In emerging, the AR interacted (reconnected) with the ambient coronal field, and magnetic loops were arranged radially with the following spot that has the negative magnetic polarity as the center of the anemone structure. In Figure 5b the dark region surrounding the AR is a CH. On 22 August, when the flares/CMEs in the matter occurred, the anemone appearance somewhat changes as seen in Figure 2. This is caused by projection like many anemone ARs, while some anemone ARs keep the appearance even on the limb [*Saito et al.*, 2000].

3. Flares and CMEs

[15] Next, we focus on the two M class flares and the associated CMEs. The first flare that was M2.6 on the GOES scale, started at 00:44 UT, and peaked at 01:33 UT. The second one was M5.6 on the GOES scale, and the start and the peak times were 16:46 UT and 17:27 UT, respectively. Both are LDEs, and showed clear arcade structure. Figure 6c shows a schematic of the magnetic field during the flares. The sites of the flares were (S11° W54°) and (S12° W60°), respectively.

[16] The two flares were associated with disappearances of the Hα filaments, and Halo-type CMEs that were observed with the Large Angle Spectrometric Coronagraph (LASCO) aboard SOHO (see the SOHO/LASCO CME online catalog, http://cdaw.gsfc.nasa.gov/CME_list/) [*Yashiro et al.*, 2004]. LASCO images of the two CMEs (CME1 and CME2) are shown in Figure 7. The left panels are the LASCO C2 running difference images overlaid with EUV images taken by SOHO/EIT (195 Å), and the right panels are the LASCO

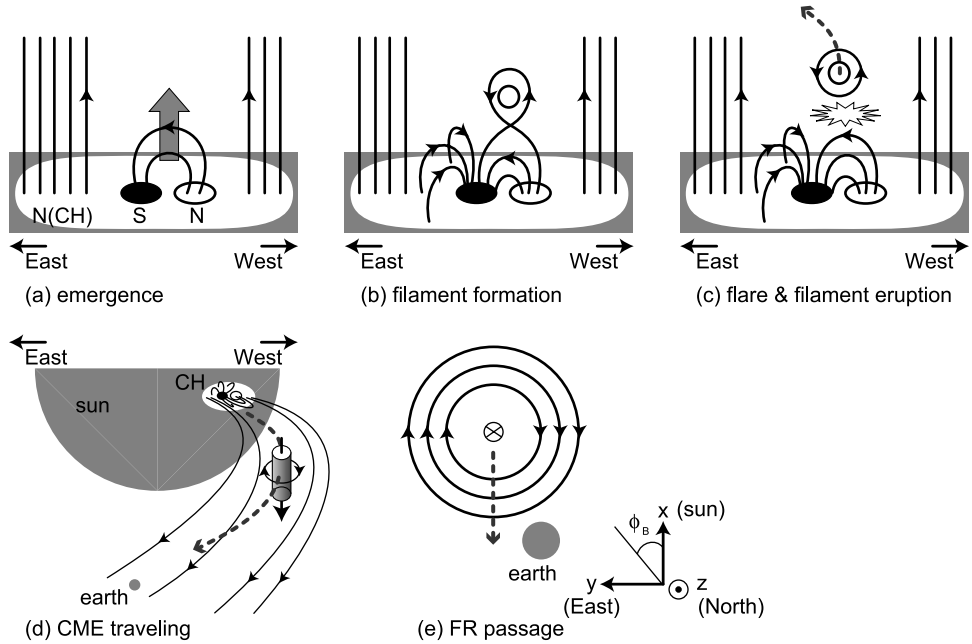

Figure 6. Schematic cartoon of AR 10798 and related flares/CMEs. (a) A magnetic flux newly emerges within a CH. (b) An anemone structure is generated, and an Hα filament is also formed above the emerged flux. (c) A magnetic reconnection occurs beneath the filament, which causes the filament eruption. The ejected plasma is bent eastward by the surrounding magnetic field with positive magnetic polarity. (d) The ejecta becomes a magnetic cloud (shown as a cylinder) that have a southward axial magnetic field and is approaching to Earth. (e) Passage of a FR and the variation of the azimuthal angle of the magnetic field ϕ_B. When a FR passes the east of Earth, ϕ_B evolutes 90–180–270 (−90) degree.

C3 running difference images. CME1 was ejected mainly to the northwest, and CME2 was to the southwest as indicated by the arrows in Figure 7. The directions were roughly consistent with the initial position of the Hα filaments (see section 2.2).

[17] It is particularly notable that the CMEs were quite fast: CME1 and CME2 had speeds of about 1200 and 2400 km s^{-1}, respectively. The speed of CME2 is ranked among the top 17 of all the 13,000 CMEs observed by SOHO/LASCO until the end of 2007. Although the time interval between the two flares/CMEs was about 16 hours, CME2 possibly caught up with CME1 before reaching 1 AU [*Gopalswamy et al.*, 2001a]. Statistically, a CME ejected with the velocity of V_{CME} have an acceleration a m s^{-2} = 2.193 − −0.0054 × V_{CME} km s^{-1} [*Gopalswamy et al.*, 2001b], and the expected accelerations for CME1 and CME2 are −4.3 and −10.8 m s^{-1} for the current case. Therefore, we estimate that the interacting between CME1 and CME2 occurred at about 1 AU (i.e., near Earth), by assuming constant accelerations for the CMEs.

[18] The interplanetary disturbance associated with the Halo-type CMEs can be followed by using interplanetary scintillation (IPS). When we see a radio source through a highly turbulent plasma associated with a CME traveling from Sun, the radio source scintillates. Therefore, such scintillations show us the electron density fluctuation caused by the CME. As an effective indicator of the electron density fluctuation, we often use g value (g) calculated from IPS data (see *Tokumaru et al.* [2000, 2003, 2005] for more details). The g value represents the variation of the electron density fluctuation in the solar wind (ΔN_e), as $g^2 \propto \int_0^\infty \Delta N_e^2 w(z) dz$, where z is a distance along the line of sight, and $w(z)$ is the IPS weighting function given by *Young* [1971]. It is normalized to the mean level of density fluctuations so that the quiet solar wind yields g value

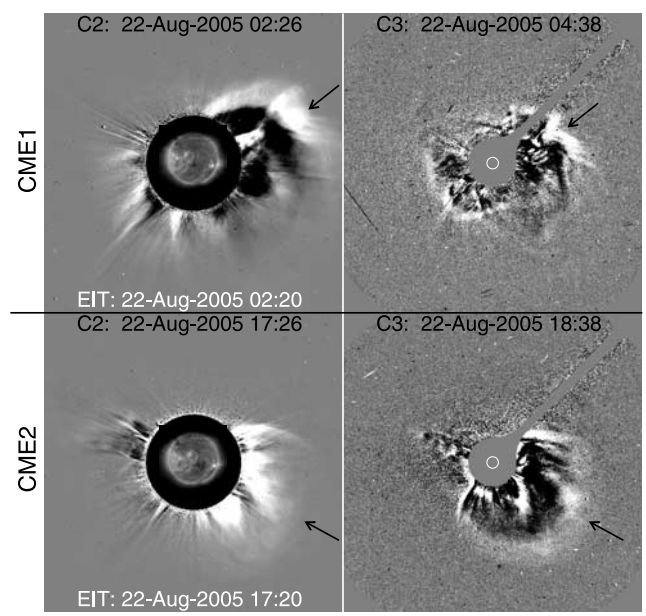

Figure 7. White light CME images obtained with SOHO/LASCO. (left) C2 running difference images for CME1/CME2 overlaid with EUV images obtained with SOHO/EIT (195Å). (right) C3 running difference images. The arrows roughly point the main part of CMEs.

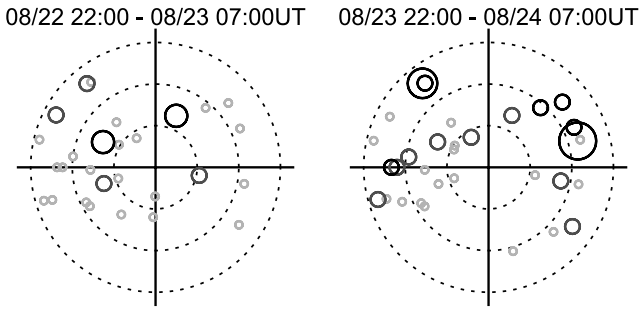

Figure 8. Daily (Japanese daytime) sky projection maps of g values obtained with IPS observations at STEL Nagoya University. In each map, the center corresponds to Sun center, and the dotted cocentric circles are constant radii contours from Sun drawn at 0.3, 0.6, and 0.9 AU. Solid circles indicate the points of the closest approach to Sun (P points) on the line of sight where g value data were obtained (P point approximation). Dark gray and black circles represent the locations where the g values are larger than 1.5 and 2.0, respectively.

around unity, and the enhancement ($g > 1$) shows the passing of a turbulent plasma.

[19] We examined the g values taken with IPS at Solar-Terrestrial Environment Laboratory (STEL), Nagoya University [*Kojima and Kakinuma*, 1990; *Asai et al.*, 1995; *Tokumaru et al.*, 2000]. Figure 8 shows the daily (Japanese daytime) sky projection maps of the g values. In each map, the center corresponds to the location of Sun, and dotted cocentric circles are constant radii contours from Sun drawn at 0.3, 0.6, and 0.9 AU. The solid circles indicate the points of the closest approach to Sun (P points) on the line of sight where g value were obtained (P point approximation). The locations of the stronger g values are emphasized by colors and sizes of the circles. The dark gray and the black circles represent the locations where the g values are larger than 1.5 and 2.0, respectively.

[20] In both panels of Figure 8 we can see density fluctuations that were caused by the two Halo CMEs, while we cannot distinguish the individual CMEs discretely due the low spatial resolution of IPS. The front of the disturbance, which was caused by CME1, reached about 0.4 and 0.8 AU on August 23 and 24, respectively. CME1 is well decelerated, and the speed is about 700 km s^{-1}. These fluctuations are distributed roughly in all direction.

4. Interplanetary Disturbance

[21] Here, we investigate in more detail why a strong disturbance with a magnetic field of about −50 nT arrived at Earth. As we mentioned above (see section 4), CME2 probably caught up with CME1, and therefore, disturbance is regarded as a merged product of CME1 and CME2, although the interaction was not directly observed.

[22] Figure 9 shows a 7-hour interval corresponding to the geo-effective part of the interplanetary disturbance from Geotail. The top four panels present the magnetic field in GSE coordinates obtained by the Magnetic Field Experiment (MGF [*Kokubun et al.*, 1994]). The magnitude $|B|$ and the x (B_x), y (B_y), and z components (B_z) of the magnetic field are shown. The fifth panel shows the ion velocity V_x observed with the Low Energy Particle Experiment (LEP [*Mukai et al.*, 1994]). The bottom panel shows the electron density N_e observed by the Plasma Wave Instrument (PWI [*Matsumoto et al.*, 1994]). The density reached so high that the counts of the particle detectors onboard Geotail (and probably ACE as well) were saturated, and therefore, it is underestimated during the strong disturbance. To avoid the underestimation of the density, we simply traced local enhancements of the electrostatic noise that appears in the dynamic spectra of the electric field as have been carried out elsewhere (see, e.g., Figure 4 of *Terasawa et al.* [2005]). Although the measurement also have a uncertainty, it is more accurate than that by particle measurement experiments, since the counts were not saturated.

[23] A flux rope (FR) structure can be identified by the smooth rotation of the magnetic field from 09:15 to 11:15 UT as shown by the vertical dashed lines in Figure 9. It is notable that the 2 hours duration of this FR was extremely short compared to the typical duration of about 20 hours [*Lepping et al.*, 2003; *Gopalswamy*, 2006]. The local velocities of the FR is 650 km s^{-1}, as will be discussed below. We estimated the radial size of the FR to be about 0.03 AU, by multiplying the local velocity by the 2 hours duration. This value is also extremely small compared with typical ones of 0.2–0.3 AU [*Forsyth et al.*, 2006]. This FR showed the smooth rotation from positive to negative B_y, a negative B_z peak in the middle of the B_y rotation, and relatively small B_x component. These can be roughly explained by the passage of a right-handed flux rope with the southward pointing axis field, which is consistent with the magnetic field configuration of the associated Hα filaments. The largest geomagnetic storm of cycle 23 that occurred on 20 November 2003 was associated with a similar FR [*Gopalswamy et al.*, 2005].

[24] About 15 min before the front edge of the FR (i.e., at about 09:00 UT), a solar wind discontinuity is identified by the sudden increases in the magnetic field, solar wind speed, and density as shown by the vertical solid line. From the variation of velocity distribution function, we confirmed an abrupt increase of temperature (not shown) there, and concluded that the discontinuity is a shock. We call the discontinuity as the "second shock," and the "first shock" is for the one observed at the beginning of the event as shown with the dashed line in Figure 1 and the vertical solid line at about 06:15 UT in Figure 9.

[25] The extremely strong southward magnetic field, the unusual short duration of the FR (2 hours), and very small separation between the second shock and the FR front (15 min) can be naturally explained, if we regard the disturbance as the product of very fast shock wave associated with CME2 interacting with the slower body of CME1 in traveling to Earth. Therefore, CME2 suffered from a strong deceleration, which implies that there was a great compression of the interplanetary medium in front of CME2. In this case the first and the second shocks are thought to be associated with CME1 and CME2, respectively.

[26] The local velocities of the first and the second shocks are measured by the positional relation between the ACE and Geotail satellites, and therefore, we can roughly estimate their accelerations (decelerations). ACE and Geotail were located at (223.7, 10.6, 4.5) and (12.9, 25.7, 1.9) R_E (= 6378 km) at

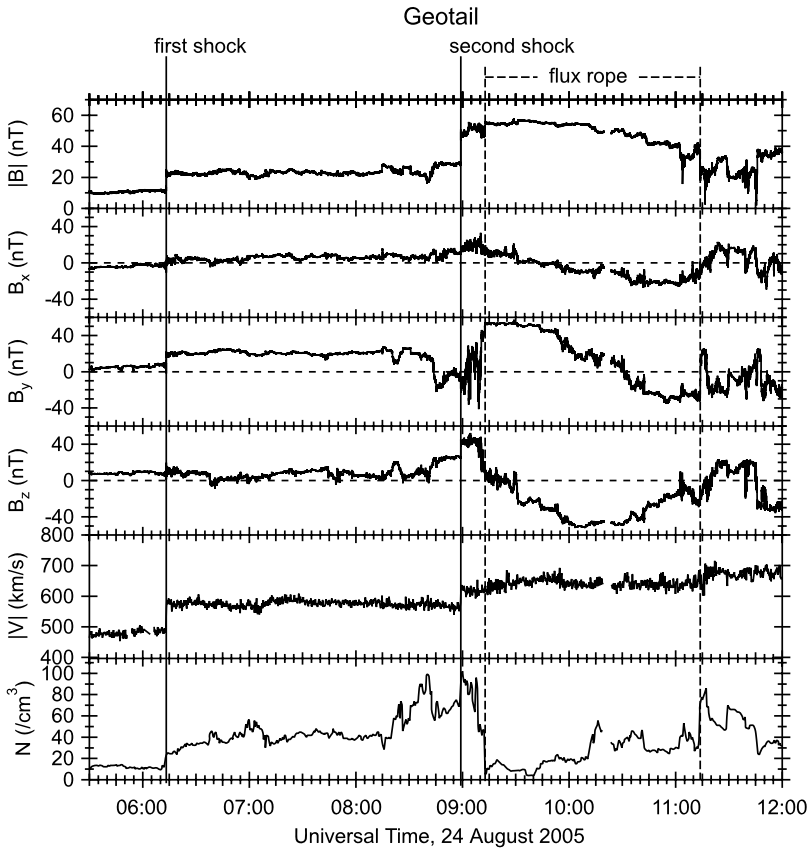

Figure 9. Geotail observation of the interplanetary disturbance on 24 August 2005. (top to bottom) Magnitude and X, Y, and Z components in GSE coordinate of the magnetic field (MGF experiment), ion velocity (LEP/SWI experiment), and electron density (PWI/SFA). The vertical solid lines show the shocks (the first and the second shocks). The vertical dashed lines show the flux rope.

09:00 UT on 24 August 2005 in GSE coordinate system, respectively. As already mentioned, CME1 and CME2 were ejected with velocities of about 1200 and 2400 km s^{-1}, at intervals of 16 hours. On the other hand, the local velocities of the first and the second shocks are 650 and 710 km s^{-1}, respectively, and the time separation between them is reduced to only about 3 hours. Assuming the constant accelerations, they are estimated to be -3.2 and -13 m s^{-2}. As we calculated above, the accelerations for CME1 and CME2 are statistically expected to be -4.3 and -10.8 m s^{-1}. The additional deceleration of CME2 also indicates that it interacted with slower CME1 and compressed the interplanetary medium there.

5. Summary and Discussions

[27] In order to make clear the importance of an AR that emerged in a CH to generate geo-effective flares/CMEs, we examined the evolution of the AR NOAA 10798, the solar events associated with a geomagnetic storm that occurred on 24 August 2005, and the related interplanetary disturbances. The summary of the features of the AR and the events is as follows: (1) Highly twisted and complex magnetic flux emerged within a small CH on 18 August 2005, which was named NOAA 10798; (2) An anemone type structure was generated, and Hα filaments that had southward axial fields were formed on 21 August 2005; (3) Two halo CMEs associated with M class flares occurred on 22 August 2005; (4) The CME speeds were fast, especially the second one recorded 2400 km s^{-1}; (5) The interplanetary disturbances with strong southward magnetic field of about -50 nT and strong compression of plasma were produced.

[28] The CMEs were particularly geo-effective, and the minimum Dst index was -216 nT. The reasons for the CMEs to be so geo-effective were the high speeds of the two CMEs and their interaction as well as the CMEs traveled directly toward Earth. For the current case, the speed of CME2 was faster and pushed the slower CME1, which led to a unusual strong compression of the plasma at the front of CME2.

[29] The high speeds of the CMEs are more notable. The AR was large and very complex, and violated the Hale-Nicholson's magnetic polarity law. These reverted polarity ARs are statistically favorable to produce large flares. However, it is suspicious whether just the violation of the Hale-Nicholson's law is responsible for high speed CMEs of about 2000 km s^{-1}, and it should be quantitatively and statistically clarified in the future. In this paper we suggest that the fast CMEs are probably a consequence of the eruption inside a CH from an anemone AR. This is consistent with the association between fast Halo CMEs and CHs as reported before [*Verma*, 1998; *Liu and Hayashi*, 2006; *Liu*, 2007].

[30] Eruptive activities of anemone ARs are usually low [*Asai et al.*, 2008], and often confined to small-scale activities inside CHs that appears to be SXR bright points. In some cases, anemone ARs can produce large SXR coronal jets [*Shibata et al.*, 1994b; *Vourlidas et al.*, 1996; *Kundu et al.*, 1999; *Alexander and Fletcher*, 1999]. This is because the situation of an emergence of a magnetic flux within a CH is suitable for magnetic reconnection with the surrounding field to generate SXR coronal jets and/or Hα surges [*Yokoyama and Shibata*, 1995, 1996]. *Wang* [1998] indicates the possibility that even polar plumes are associated with jets from anemone ARs at high latitudes. Anemone ARs are related to nonradial coronal streamers emanating from magnetically high latitudes [*Saito et al.*, 2000]. The relation between anemone ARs and fast solar winds have also been paid attentions to [*Takahashi et al.*, 1994; *Saito et al.*, 1994; *Wang*, 1998]. *Saito et al.* [2000] further discussed the rotational reversing model and the triple dipole model to explain the reversal of the solar surface magnetic field, and anemone ARs play an important role in this. This model implies that anemone ARs are more conspicuous in the decaying phase of a solar cycle as in the case of AR NOAA 10798.

[31] On the other hand, the deflection of CMEs eastward by the interplanetary fields effectively worked in the current case as shown in the Figure 6d. As *Wang et al.* [2006] pointed out, the faster CMEs are deflected more eastward, and therefore, the AR NOAA 10798 generated geo-effective CMEs, although it was quite close to the southwest limb. The azimuthal angle of the magnetic field measured from the x axis ϕ_B (= $\arctan(B_y/B_x)$) changed 90°–180°–270° (−90°) during the passage of the FR, which is consistent with the guess that the deflection of the CMEs were so strong that the axis of the FR passed through the east of Earth. This is also consistent with the fact that the flares in the next rotation (and renamed as NOAA 10808) did not affect the magnetosphere so much [*Wang et al.*, 2006; *Nagashima et al.*, 2007]. Furthermore, the extremely short duration of FR and the missing of CME1 (see Figure 9) are possibly explained by the skimming encounter with the CMEs due to the strong deflection.

[32] The nature of the interplanetary disturbances and their impact on the magnetosphere strongly depend on the features of emergence and evolution of an AR and the relation with the surrounding magnetic field. In this work we succeeded to follow in detail the evolution of the AR and the large geomagnetic storm resulting from eruptions in the AR. The reconstruction of the proposed scenario using numerical simulations will be attempted in the future.

[33] **Acknowledgments.** We first acknowledge anonymous referees for their useful comments and suggestions. We wish to thank J. Kozyra, K. Hayashi, N. V. Nitta, V. Yurchyshyn, and B. J. Thompson for fruitful discussions and their helpful comments. This work was supported by the Grant-in-Aid for the Global COE Program "The Next Generation of Physics, Spun from Universality and Emergence" from the Ministry of Education, Culture, Sports, Science and Technology (MEXT) of Japan. This work was also supported by the Grant-in-Aid for Creative Scientific Research "The Basic Study of Space Weather Prediction" (17GS0208, Head Investigator: K. Shibata) from the Ministry of Education, Science, Sports, Technology, and Culture of Japan. This work was partially carried out by the joint research program of the Solar-Terrestrial Environment Laboratory, Nagoya University. We would like to acknowletge all the members of the Geotail/PWI, LEP, and MGF for providing the data. We would like to thank WDC for Geomagnetism, Kyoto Dst index service. Our thanks also go to the SMART teams of Hida Observatory, Kyoto University, Big Bear Solar Observatory, and Meudon Observatoire de Paris, Section de Meudon, for letting us use the Hα data. We made extensive use of SOHO, and ACE Data Center. M.O. was supported by the Grant-in-Aid for JSPS Postdoctoral Fellows for Research Abroad.

[34] Amitava Bhattacharjee thanks the reviewers for their assistance in evaluating this paper.

References

Alexander, D., and L. Fletcher (1999), High-resolution observations of plasma jets in the solar corona, *Sol. Phys.*, *190*, 167, doi:10.1023/A:1005213826793.

Asai, A., K. Shibata, T. T. Ishii, and N. Gopalswamy (2006), Anemone structure of NOAA 10798 and geo-effective flares/CMEs, paper presented at CSWM Workshop, Yokohama, Japan. (Available at http://workshops.jhuapl.edu/s1/conf/solar-wind/asai-01/asai-01.pdf)

Asai, A., K. Shibata, H. Hara, and N. V. Nitta (2008), Characteristics of anemone active regions appearing in coronal holes observed with Yohkoh soft X-ray telescope, *Astrophys. J.*, *673*, 1188, doi:10.1086/523842.

Asai, K., Y. Ishida, M. Kojima, K. Maruyama, H. Misawa, and N. Yoshimi (1995), Multi-station system for solar wind observations using the interplanetary scintillation method, *J. Geomagn. Geoelectr.*, *47*, 1107.

Bruzek, A. (1967), On arch-filament systems in spotgoups, *Sol. Phys.*, *2*, 451, doi:10.1007/BF00146493.

Delaboudiniére, J.-P., et al. (1995), EIT: Extreme-Ultraviolet Imaging Telescope for the SOHO mission, *Sol. Phys.*, *162*, 291, doi:10.1007/BF00733432.

Domingo, V., B. Fleck, and A. I. Poland (1995), The SOHO mission: An overview, *Sol. Phys.*, *162*, 1, doi:10.1007/BF00733425.

Forsyth, R. J., et al. (2006), ICMEs in the inner heliosphere: Origin, evolution and propagation effects, *Space Sci. Rev.*, *123*, 383, doi:10.1007/s11214-006-9022-0.

Gopalswamy, N. (2006), Properties of interplanetary coronal mass ejections, *Space Sci. Rev.*, *124*, 145, doi:10.1007/s11214-006-9102-1.

Gopalswamy, N., S. Yashiro, M. L. Kaiser, R. A. Howard, and J.-L. Bougeret (2001a), Radio signatures of coronal mass ejection interaction: Coronal mass ejection cannibalism?, *Astrophys. J.*, *548*, L91, doi:10.1086/318939.

Gopalswamy, N., A. Lara, S. Yashiro, M. L. Kaiser, and R. A. Howard (2001b), Predicting the 1-AU arrival times of coronal mass ejections, *J. Geophys. Res.*, *106*(A12), 29,207, doi:10.1029/2001JA000177.

Gopalswamy, N., S. Yashiro, G. Michalek, H. Xie, R. P. Lepping, and R. A. Howard (2005), Solar source of the largest geomagnetic storm of cycle 23, *Geophys. Res. Lett.*, *32*, L12S09, doi:10.1029/2004GL021639.

Gopalswamy, N., S. Yashiro, and S. Akiyama (2007), Geoeffectiveness of halo coronal mass ejections, *J. Geophys. Res.*, *112*, A06112, doi:10.1029/2006JA012149.

Gosling, J. T., S. J. Bame, D. J. McComas, and J. L. Phillips (1990), Coronal mass ejections and large geomagnetic storms, *Geophys. Res. Lett.*, *17*, 901.

Hale, G. E., F. Ellerman, S. B. Nicholson, and A. H. Joy (1919), The magnetic polarity of Sun-spots, *Astrophys. J.*, *49*, 153, doi:10.1086/142452.

Ishii, T. T., H. Kurokawa, and T. T. Takeuchi (2000), Emergence of twisted magnetic-flux bundles and flare activity in a large active region, NOAA 4201, *Publ. Astron. Soc. Jpn.*, *52*, 337.

Kataoka, R., and Y. Miyoshi (2006), Flux enhancement of radiation belt electrons during geomagnetic storms driven by coronal mass ejections and corotating interaction regions, *Space Weather*, *4*, S09004, doi:10.1029/2005SW000211.

Kojima, M., and T. Kakinuma (1990), Solar cycle dependence of global distribution of solar wind speed, *Space Sci. Rev.*, *53*, 173.

Kokubun, S., T. Yamamoto, M. H. Acuna, K. Hayashi, K. Shiokawa, and H. Kawano (1994), The GEOTAIL magnetic-field experiment, *J. Geomagn. Geoelectr.*, *46*, 7.

Kundu, M. R., A. Nindos, J.-P. Raulin, K. Shibasaki, S. M. White, N. Nitta, K. Shibata, and M. Shimojo (1999), A microwave study of coronal ejecta, *Astrophys. J.*, *520*, 391, doi:10.1086/307454.

Kurokawa, H., T.-J. Wang, and T. T. Ishii (2002), Emergence and drastic breakdown of a twisted flux rope to trigger strong solar flares in NOAA active region 9026, *Astrophys. J.*, *572*, 598, doi:10.1086/340305.

Lepping, R. P., D. B. Berdichevsky, A. Szabo, C. Arqueros, and A. J. Lazarus (2003), Profile of an average magnetic cloud at 1 au for the quiet solar phase: Wind observations, *Sol. Phys.*, *212*, 425.

Liu, Y. (2007), Halo coronal mass ejections and configuration of the ambient magnetic fields, *Astrophys. J.*, *654*, L171, doi:10.1086/511385.

Liu, Y., and K. Hayashi (2006), The 2003 October–November fast halo coronal mass ejections and the large-scale magnetic field structures, *Astrophys. J.*, *640*, 1135, doi:10.1086/500290.

López Fuentes, M. C., P. Démoulin, C. H. Mandrini, A. A. Pevtsov, and L. van Driel-Gesztelyi (2003), Magnetic twist and writhe of active

regions: On the origin of deformed flux tubes, *Astron. Astrophys.*, *397*, 305, doi:10.1051/0004-6361:20021487.

Low, B. C., and J. R. Hundhausen (1995), Magnetostatic structures of the solar corona. 2: The magnetic topology of quiescent prominences, *Astrophys. J.*, *443*, 818, doi:10.1086/175572.

Manoharan, P. K., N. Gopalswamy, S. Yashiro, A. Lara, G. Michalek, and R. A. Howard (2004), Influence of coronal mass ejection interaction on propagation of interplanetary shocks, *J. Geophys. Res.*, *109*, A06109, doi:10.1029/2003JA010300.

Martin, S. F. (1973), The evolution of prominences and their relationship to active centers, *Sol. Phys.*, *31*, 3, doi:10.1007/BF00156070.

Matsumoto, H., I. Nagano, R. R. Anderson, H. Kojima, K. Hashimoto, M. Tsutsui, T. Okada, I. Kimura, Y. Omura, and M. Okada (1994), Plasma wave observations with GEOTAIL spacecraft, *J. Geomagn. Geoelectr.*, *46*, 59.

Mukai, T., S. Machida, Y. Saito, M. Hirahara, T. Terasawa, N. Kaya, T. Obara, M. Ejiri, and A. Nishida (1994), The low energy particle (LEP) experiment onboard the GEOTAIL satellite, *J. Geomagn. Geoelectr*, *46*, 669.

Munro, R. H., J. T. Gosling, E. Hildner, R. M. MacQueen, A. I. Poland, and C. L. Ross (1979), The association of coronal mass ejection transients with other forms of solar activity, *Sol. Phys.*, *61*, 201.

Nagashima, K., H. Isobe, T. Yokoyama, T. T. Ishii, T. J. Okamoto, and K. Shibata (2007), Triggering mechanism for the filament eruption on 2005 September 13 in active region NOAA 10808, *Astrophys. J.*, *668*, 533, doi:10.1086/521139.

Rust, D. M. (1994), Spawning and shedding helical magnetic fields in the solar atmosphere, *Geophys. Res. Lett.*, *21*, 241.

Saito, T., Y. Kozuka, S. Tsuneta, and S. Minami (1994), Rotational reversing model and triple dipole model as substantiated by Yohkoh SXT data, in *Proceedings of International Symposium on the Yohkoh Scientific Results, X-Ray Solar Physics from Yohkoh*, edited by Y. Uchida, T. Watanabe, K. Shibata, and H. S. Hudson, p. 211, Universal Acad., Tokyo.

Saito, T., K. Shibata, K. P. Dere, and S. Numazawa (2000), Non-radial unipolar coronal streamers in manetically high latitudes and radial bipolar streamers at the magnetic equator of the Sun, *Adv. Space Res.*, *26*, 807.

Scherrer, P. H., et al. (1995), The Solar Oscillations Investigation—Michelson Doppler Imager, *Sol. Phys.*, *162*, 129, doi:10.1007/BF00733429.

Sheeley, N. R., Jr., J. D. Bohlin, G. E. Brueckner, J. D. Purcell, V. Scherrer, and R. Tousey (1975a), XUV observations of coronal magnetic fields, *Sol. Phys.*, *40*, 103.

Sheeley, N. R., Jr., J. D. Bohlin, G. E. Brueckner, J. D. Purcell, V. E. Scherrer, and R. Tousey (1975b), The reconnection of magnetic field lines in the solar corona, *Astrophys. J.*, *196*, 129.

Sheeley, N. R., Jr., J. W. Harvey, and W. C. Feldman (1976), Coronal holes, solar wind streams, and recurrent geomagnetic disturbances—1973–1976, *Sol. Phys.*, *49*, 271.

Shibata, K., N. Nitta, R. Matsumoto, T. Tajima, T. Yokoyama, T. Hirayama, and H. Hudson (1994a), Two types of interaction between emerging flux and coronal magnetic field, in *Proceedings of International Symposium on the Yohkoh Scientific Results, X-Ray Solar Physics from Yohkoh*, edited by Y. Uchida, T. Watanabe, K. Shibata, and H. S. Hudson, p. 29, Universal Acad., Tokyo.

Shibata, K., N. Nitta, K. T. Strong, R. Matsumoto, T. Yokoyama, T. Hirayama, H. Hudson, and Y. Ogawara (1994b), A gigantic coronal jet ejected from a compact active region in a coronal hole, *Astrophys. J.*, *431*, L51, doi:10.1086/187470.

Shibata, K., et al. (2007), Chromospheric anemone jets as evidence of ubiquitous reconnection, *Science*, *318*, 1591, doi:10.1126/science.1146708.

Takahashi, T., T. Saito, K. Shibata, Y. Kozuka, S. Minami, and Y. Mori (1994), Structure of the soft X-ray corona and its effect to the Earth quadrupole type and sea anemone type, in *Proceedings of International Symposium on the Yohkoh Scientific Results, X-Ray Solar Physics from Yohkoh*, edited by Y. Uchida, T. Watanabe, K. Shibata, and H. S. Hudson, p. 305, Universal Acad., Tokyo.

Terasawa, T., et al. (2005), Determination of shock parameters for the very fast interplanetary shock on 29 October 2003, *J. Geophys. Res.*, *110*, A09S12, doi:10.1029/2004JA010941.

Tian, L., D. Alexander, Y. Liu, and J. Yang (2005), Magnetic twist and writhe of δ active regions, *Sol. Phys.*, *229*, 63, doi:10.1007/s11207-005-3524-x.

Tokumaru, M., M. Kojima, K. Fujiki, and A. Yokobe (2000), Three-dimensional propagation of interplanetary disturbances detected with radio scintillation measurements at 327 MHz, *J. Geophys. Res.*, *105*(A5), 10,435, doi:10.1029/2000JA900001.

Tokumaru, M., M. Kojima, K. Fujiki, M. Yamashita, and A. Yokobe (2003), Toroidal-shaped interplanetary disturbance associated with the halo coronal mass ejection event on 14 July 2000, *J. Geophys. Res.*, *108*(A5), 1220, doi:10.1029/2002JA009574.

Tokumaru, M., M. Kojima, K. Fujiki, M. Yamashita, and D. Baba (2005), Interplanetary consequences caused by the extremely intense solar activity during October–November 2003, *J. Geophys. Res.*, *110*, A01109, doi:10.1029/2004JA010656.

Tousey, R., et al. (1973), A preliminary study of the extreme ultraviolet spectroheliograms from Skylab, *Sol. Phys.*, *33*, 265, doi:10.1007/BF00152418.

Verma, V. K. (1998), On the origin of solar coronal mass ejections, *J. Ind. Geophys. Union*, *2*, 65.

Vourlidas, A., T. S. Bastian, N. Nitta, and M. J. Aschwanden (1996), Joint radio and soft X-ray imaging of an 'anemone' active region, *Sol. Phys.*, *163*, 99, doi:10.1007/BF00165459.

Wang, Y.-M. (1998), Network activity and the evaporative formation of polar plumes, *Astrophys. J.*, *501*, L145, doi:10.1086/311445.

Wang, Y.-M., X. Xue, C. Shen, P. Ye, S. Wang, and J. Zhang (2006), Impact of major coronal mass ejections on geospace during 2005 September 7–13, *Astrophys. J.*, *646*, 625, doi:10.1086/504676.

Yashiro, S., N. Gopalswamy, G. Michalek, O. C. St. Cyr, S. P. Plunkett, N. B. Rich, and R. A. Howard (2004), A catalog of white light coronal mass ejections observed by the SOHO spacecraft, *J. Geophys. Res.*, *109*, A07105, doi:10.1029/2003JA010282.

Yokoyama, T., and K. Shibata (1995), Magnetic reconnection as the origin of X-ray jets and Hα surges on the Sun, *Nature*, *375*, 42, doi:10.1038/375042a0.

Yokoyama, T., and K. Shibata (1996), Numerical simulation of solar coronal X-ray jets based on the magnetic reconnection model, *Publ. Astron. Soc. Jpn.*, *48*, 353.

Young, A. T. (1971), Interpretation of interplanetary scintillations, *Astrophys. J.*, *168*, 543, doi:10.1086/151108.

Zhang, J., et al. (2007), Solar and interplanetary sources of major geomagnetic storms ($Dst \leq -100$ nT) during 1996–2005, *J. Geophys. Res.*, *112*, A10102, doi:10.1029/2007JA012321.

A. Asai, Nobeyama Solar Radio Observatory, National Astronomical Observatory of Japan, Minamimaki, Minamisaku, Nagano 384-1305, Japan. (asai@nro.nao.ac.jp)

K. Fujiki, Solar-Terrestrial Environment Laboratory, Nagoya University, Chikusa, Nagoya, Aichi 464-8601, Japan.

N. Gopalswamy, NASA Goddard Space Flight Center, Greenbelt, MD 20771, USA.

T. T. Ishii and K. Shibata, Kwasan and Hida Observatories, Kyoto University, Yamashina, Kyoto 607-8471, Japan.

R. Kataoka, RIKEN, Wako, Saitama 351-0198, Japan.

M. Oka, Center for Space Plasma and Aeronomic Research, University of Alabama in Huntsville, Huntsville, AL 35807, USA.